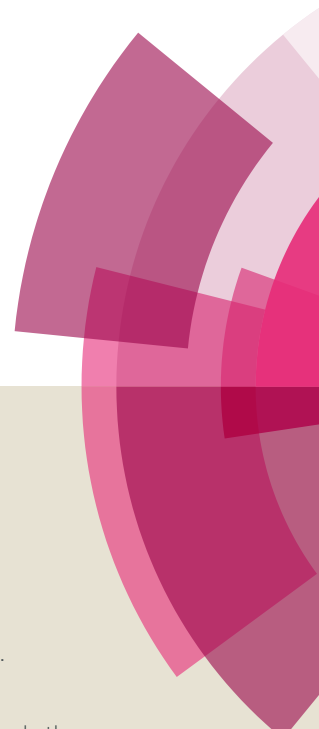
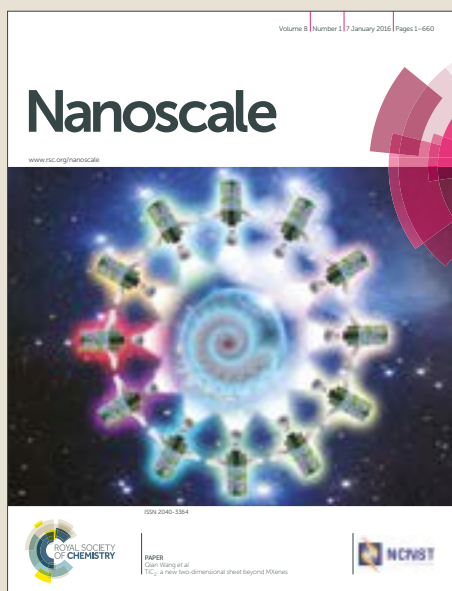


Nanoscale

Accepted Manuscript



This article can be cited before page numbers have been issued, to do this please use: S. Qi, H. Guo, J. Chen, J. Fu, C. Hu, M. Yu and Z. Wang, *Nanoscale*, 2018, DOI: 10.1039/C7NR09129J.



This is an Accepted Manuscript, which has been through the Royal Society of Chemistry peer review process and has been accepted for publication.

Accepted Manuscripts are published online shortly after acceptance, before technical editing, formatting and proof reading. Using this free service, authors can make their results available to the community, in citable form, before we publish the edited article. We will replace this Accepted Manuscript with the edited and formatted Advance Article as soon as it is available.

You can find more information about Accepted Manuscripts in the [author guidelines](#).

Please note that technical editing may introduce minor changes to the text and/or graphics, which may alter content. The journal's standard [Terms & Conditions](#) and the ethical guidelines, outlined in our [author and reviewer resource centre](#), still apply. In no event shall the Royal Society of Chemistry be held responsible for any errors or omissions in this Accepted Manuscript or any consequences arising from the use of any information it contains.



Nanoscale

PAPER

Magnetorheological elastomers enabled high sensitive self-powered tribo-sensor for magnetic field detecting

Song Qi^{a,†}, Hengyu Guo^{b,c,†}, Jie Chen^b, Jie Fu^a, Chenguo Hu^{b,*}, Miao Yu^{a,*} and Zhong Lin Wang^{c,*}

Received 00th January 20xx,
Accepted 00th January 20xx

DOI: 10.1039/x0xx00000x

www.rsc.org/

The monitoring of the magnetic field is of most significance for academic or industrial applications. In this paper, we design a self-powered magnetic-field sensor based on the magnetorheological elastomer (MRE) and triboelectric nanogenerator (TENG) that can be used for both time-varying and uniform magnetic field (UMF) sensing. This TENG-based magnetic-field sensor (TMFS) relies on contact electrification and electrostatic induction of TENG to generate a electrical signal in response to the magnetic-induced deformation of MRE without using an external power supply. Enabled by the unique sensing mechanism and excellent magnetic-induced deformation of MRE, the TMFS exhibits a fast response (20 ms) and good magnetic-field sensing performance. The TMFS with 60 wt%-MRE shows a maximum sensitivity of 16 mV/mT of the magnetic field ranging from 40 to 100 mT experimentally, and the sensitivity and detecting range of TMFS can be adjusted by several parameters of the device. Besides the contribution to the effective detection of UMF, this novel sensor provides a new idea for the magnetic-field measurements in self-powered mode.

1. Introduction

Magnetic field is a vector quantity, that is, it has both a magnitude and a direction. As the magnetic field acts as an essential role in environmental surveillance, mineral exploring, and safety monitoring, investigation on the detection of magnetic field is of greatest importance. Currently, a variety of technologies are used for the measurement of magnetic field, such as the Hall effect, fluxgate, superconducting quantum interference device (SQUID), magneto-resistance, magneto-diode or other semiconductor effects.¹⁻² Some of them are utilized for sensing the presence or variation of the field, while the others are used for detecting the magnetic field's precise value and vector property. Each of the technique possesses its unique advantage that makes it more suitable for particular situations. However, the signal generation of above detection techniques has to be supplied by external power.

Recently, self-powered technologies have caught the attention of a large number of researchers.³⁻⁵ Among them, triboelectric nanogenerator (TENG) is a burgeoning technology that can directly

collect the small-scale mechanical energy and convert it into electrical energy.⁶⁻¹⁰ Based on the coupling effect of the electrostatic induction and contact electrification,^{7, 11-12} TENG can convert almost all forms of mechanical energies, such as vibrations,¹³⁻¹⁴ rotation,¹⁵⁻¹⁷ wind,¹⁸⁻¹⁹ water flows²⁰⁻²¹ and even acoustic energy²²⁻²⁴ into electrical energy. Owing to the highly sensitive responses to mechanical triggering in TENGs, various self-powered devices and sensors based on TENG have also been designed for sensing measurement.²⁵⁻²⁶ Yang *et al.* have reported a TENG-based self-powered magnetic sensor for detecting the variation of the time-dependent magnetic field.²⁷ The results indicated that the change of magnetic field can be measured accurately by the output voltage of the sensor, and it shows a high detection sensitivity. However, this sensor is designed simply for detecting the changes in magnetic field, but it cannot be used to detect the intensity and direction of the uniform magnetic field (UMF).

As with TENG, magnetorheological elastomer (MRE) has received significant attention. The difference is that, MRE is an intelligent material, which consists of micronized magnetic particles suspended in a nonmagnetic elastic matrix.²⁸⁻³¹ With the excellent magnetic-control properties, MRE exhibits great potentials for applications in the fields of noise reduction, vibration attenuation, smart sensing, electromagnetic shielding, *etc.*³²⁻³⁶ When exposed to the UMF, the magnetic particles of MRE have a tendency to form a chain-like structure parallel to the direction of the UMF. The movement of the magnetized particles makes the deformation of MRE. The deformation of MRE in response to an external magnetic field has been studied by many researchers³⁷⁻³⁹, and several papers reported the smart devices based on the magnetic-induced

^a Key Lab for Optoelectronic Technology and Systems, Ministry of Education, College of Optoelectronic Engineering, Chongqing University, Chongqing, 400044, P. R. China..

^b Department of Applied Physics, Chongqing University, Chongqing, 400044, P. R. China..

^c Beijing Institute of Nanoenergy and Nanosystems, Chinese Academy of Sciences; National Center for Nanoscience and Technology (NCNST), Beijing, 100083, P. R. China.

[†] These authors contributed equally to this work.

* Corresponding author. Miao Yu, E-mail: yumiao@cqu.edu.cn; Chenguo Hu, E-mail: hucg@cqu.edu.cn; Zhong Lin Wang, E-mail: zhong.wang@mse.gatech.edu. Electronic Supplementary Information (ESI) available: [details of any supplementary information available should be included here]. See DOI: 10.1039/x0xx00000x

deformation of MRE.⁴⁰⁻⁴² It was proven that the magnitude of deformation is strongly depending on the magnetic field. Therefore, taking this excellent magnetic-induced deformation of MRE together with the displacement sensitivity of TENG, this work can provide a useful measuring mean for the detection of UMF.

Herein, in order to measure the intensity and direction of the UMF, this paper develops a self-powered sensor based on TENG to detect the magnetic-induced deformation of the MRE. The structure and mechanism of the TMFS have been illustrated in detail. The material properties of MRE and output signals of the sensor have also been systematically studied. Besides, the influences of the MRE, UMF and the structural parameters of TMFS on the output voltage of the sensor were discussed, and relevant physical mechanism was analyzed. These results revealed that the TMFS had considerable potential application for magnetic field measurements in self-powered mode.

2. Experimental section

2.1 MRE film fabrication.

A schematic diagram of the fabrication process of the MRE film is shown in Fig. 1a. MRE was fabricated by mixing carbonyl iron particles (CIPs, type:CN; size distribution: 1–8 μm ; provided by BASF) into the silicone rubber (Ecoflex 0020; provided by Smooth-On, Inc.) at different mass fraction (20 wt%, 30 wt%, 40 wt%, 50 wt%, 60 wt%). The CIPs were firstly mixed into the uncured liquid silicone rubber by mechanical stirring and via

ultrasonication for 1h to ensure the particles' uniform distribution. Subsequently, the cross-linker of the silicone rubber was added into the aforementioned suspension by mechanical stirring for 30 minutes. Deserve to be mentioned, the resulting mixture was degassed for 20 minutes in a vacuum oven at 30 $^{\circ}\text{C}$ so as to remove the bubbles. Finally, the mixture was then placed into acrylic mould and formed into films with different thickness.

2.2 Device fabrication.

Fig. 1c illustrates the structure of the TMFS, which mainly consists of upper and lower parts. The lower part is the deformation component comprises of MRE and latex film over its surface. To ensure that the central portion of the MRE is free to deform, the MRE was cut in disc forms with 5 mm in diameter and attached to the acrylic ring plate. In addition, a latex film was attached to the MRE film for acting as the positive tribo-material. The upper part is the TENG component consists of Fluorinated ethylene propylene (FEP), Poly(ethylene terephthalate (PET) and copper. It's worth mentioning that the TENG fabrication process started from the preparation of several circular film components. The FEP, PET and copper films were stacked together in turn, and these multi-layer structures were attached to the acrylic plate. In order to enlarge and ensure the deformation direction of MRE, another MRE film was totally fixed onto the acrylic plate of the TENG component, as shown in Fig. 1d. Finally, the as-prepared TENG layers were assembled in parallel with the deformation element, and the TENG layers received the support of four springs and bolts. The gap between the upper part and lower part is 1.5 mm, and it can be adjusted by the screw cap.

2.3 Materials characterization and output measurement.

The morphologies of the MRE and FEP were characterized via scanning electron microscopy (SEM; MIRA3TESCAN). The mechanical property of MRE was measured by CTM2100 materials test machine (CTM, Shanghai, People's Republic of China). The output signals of the TENG unit were measured by a voltage preamplifier (Keithley 6514 System Electrometer). The software platform was constructed based on LabVIEW, which was capable of realizing real-time data acquisition and analysis.

3. Results and discussion

3.1 Mechanism of the Sensor.

Fig. 1 shows the structure design of the TMFS, the measurement of UMF can be achieved by the electric signal of TENG induced from the magnetic-induced deformation of MRE. Fig.1b shows the photograph of MRE film and designed TMFS. The flexible MRE film has the sensitive magnetic-induced deformation property, and the deformation will make the positively charged latex film close to the negatively charged FEP, as shown in Fig.1d. The electrostatic induction will cause the change in the open-circuit voltage across the two electrodes, and the magnitude of the electric output signal is indicative of the local magnetic field. The mechanisms of the magnetic-induced deformation of MRE and TENG will be discussed details in the following sections.

3.1.1 Mechanism of the magnetic-induced deformation of MRE under UMF.

The CIPs were distributed randomly in the matrix of

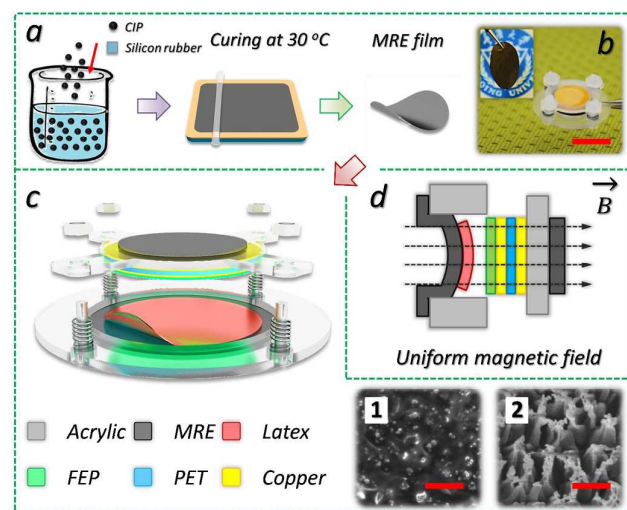


Fig. 1. Structure design of the TMFS. (a) Preparation process of the MRE film. (b) Photograph of MRE film and designed TMFS, the scale bar is 5 mm. (c) Schematic illustration of the structure of the TMFS, which consists of upper and lower parts. The lower part is the deformation element-contained MRE and latex films, and the upper part consists of FEP, PET and copper. Insets 1 and 2 show the SEM image of MRE and FEP surface, the scale bar is 50 μm and 500 nm respectively. (d) Schematic diagram of the deformation mechanism of the TMFS under UMF.

isotropic MRE, as shown in inset 1 of Fig. 1c. Fig. S1 shows the magnetization curves of CIP and MRE, which indicated that both of them have excellent soft magnetic properties. It ensures the excellent monitoring repeatability of TMFS. Fig. S2 shows the magnetic simulation of representative volume element (RVE) of MRE. The permeability of the CIPs is much greater than that of the matrix, resulting in a larger magnetic flux density in the CIPs, as the Fig.S2a shows. It can be seen that the magnetic flux density also depends on the particle size and spacing. Fig.S2b shows magnetic stress tensor generated on the particle surface, and the magnitude of the tensor is related to the direction of the magnetic field. These directional stress tensors make the uniformly dispersed CIPs tend to form a chain structure parallel to the direction of the magnetic field, which causes the magnetic-induced deformation of MRE. In order to ensure the deformation only occurs along the vertical direction, the edge of the rounded MRE film is bonded with the acrylic ring plate. Besides, to enlarge the deformation of MRE, another MRE film is totally fixed on the acrylic plate of the TENG unit. This totally fixed MRE can provide an additional magnetic attraction for the deformable MRE film, which could improve the sensitivity of the sensor. To explain the magnetic-induced deformation response of the MRE film from physical mechanisms, a theoretical model is proposed based on linear elastic theory of the MRE film. To simplify, all CIPs are assumed to be homogeneous spheres that can be treated as identical dipoles and the distances between particles are equal. Besides, we assume the magnetized fixed MRE as a uniform plate magnet and ignore the mutual magnetic induction between the two MREs, as the Fig. 2a shows. In an external magnetic field

\mathbf{H}_0 , the CIPs of deformable MRE become magnetized and additionally attracted by the magnetized fixed MRE. The magnetic moment \mathbf{m}_m of the magnetized fixed MRE under the magnetic field \mathbf{H}_0 is:

$$\mathbf{m}_m = \mathbf{M} \cdot V_i \quad (1)$$

Here, \mathbf{M} and V_i are the magnetization intensity and volume of the fixed MRE respectively. With a magnetic moment \mathbf{m}_m , the fixed MRE could induce an inhomogeneous stray field \mathbf{H}_i in the surrounding space, and the \mathbf{H}_i is mainly depending on the permeability and volume of the fixed MRE, external magnetic field \mathbf{H}_0 and the distances between the space point and the fixed MRE. To simplify, we assume that the \mathbf{H}_i is a uniform magnetic field parallel to \mathbf{H}_0 for a single magnetic dipole. Hence, the \mathbf{H}_i can be expressed as:

$$\mathbf{H}_i = \alpha f(\lambda) \mathbf{H}_0 \quad (2)$$

Here, α is a constant which depended on the permeability, susceptibility, shape of MRE, etc. $f(\lambda)$ is the function of the distances λ between the space point and the fixed MRE. For the deformable MRE, due to the large demagnetizing factor of CIPs, it can be assumed that the magnetic moment \mathbf{m}_p of the particles in deformable MRE depends linearly on the magnetic field strength \mathbf{H} ⁴³, here $\mathbf{H} = \mathbf{H}_0 + \mathbf{H}_i$:

$$\mathbf{m}_p = \frac{4\pi\mu_0\mu_1\chi \cdot r^3}{3} \mathbf{H} \quad (3)$$

Where r is the particle radius, μ_0 and μ_1 is the vacuum permeability and permeability of MRE respectively, χ is the susceptibility of CIPs. Under a magnetic field, the \mathbf{m}_p of dipoles became oriented and to form a structure that is ordered under the shape of that in Fig. 2a. The orientation of the \mathbf{m}_p is parallel to the orientation of \mathbf{H} . With increasing magnetic field, both percentage of rotated particles and the rotation angle of each particle increase, which results in the elongation of the MRE.⁴⁴ The magnetized particles tend to attract to each other, which would lead to the formation of an ordered structure with the particles aligning along the magnetic field direction. Then, under magnetic field \mathbf{H} , the force (attraction) between two magnetic dipoles can be expressed as⁴⁵:

$$F' = \frac{2\pi\mu_0 r^6 H^2}{d^4} \quad (4)$$

where μ_0 is the vacuum permeability, H is the quantity of \mathbf{H} , d is the distance between the centers of the magnetic dipoles. Under the action of F' , according to Hooke's law, the elastic medium reacts with the elastic force:

$$F'_{el} = k\Delta d \quad (5)$$

In which k and Δd is the coupling constant and strain between two neighboring particles. Assuming the dipole moment is kept constant when the MRE is deformed. At balance, between the two forces, there takes place the equality:

$$F' = \frac{2\pi\mu_0 r^6 H^2}{d^4} = F'_{el} = k\Delta d \quad (6)$$

From the Eq. (2) and Eq. (6), we can deduce that the external magnetic field strength H_0 can be expressed as:

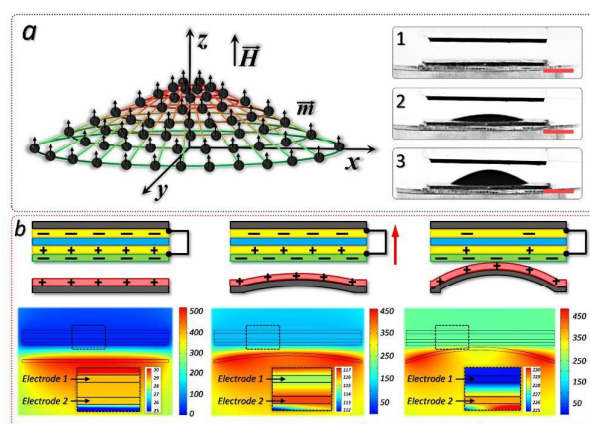


Fig. 2. Schematic diagrams of working mechanisms of the TMFS. (a) Schematic illustration of the structure with magnetic dipoles in the elastic matrix of MRE film under a UMF: \vec{m} is magnetic dipole; \vec{H} is magnetic field vector; Oxyz coordinates axis system. Insets 1, 2 and 3 show the photographs of the magneto-deformation of MRE under the 0 mT, 100 mT and 200 mT respectively, the scale bar is 1 mm. (b) Schematic illustrations of the charge distributions of TENG under the different magnetic field strength, indicating the relationship between the magneto-deformation of MRE and the charge distribution of TENG. The second half of the illustration shows the numerical calculations of the potential distribution across the electrodes of the TENG under the different magnetic field strength, as evaluated by COMSOL.

$$H_0 = \frac{d^2}{r^3(\alpha f(\lambda)+1)} \sqrt{\frac{k\Delta d}{2\pi\mu_0}} \quad (7)$$

Assuming the $f(\lambda)$ is a constant. Eq. (7) could be simplified as:

$$H_0 \approx \rho\sqrt{\Delta d} \quad (8)$$

Where $\rho = \frac{d^2}{r^3(\alpha f(\lambda)+1)} \sqrt{\frac{k}{2\pi\mu_0}}$ is a constant. From the Eq. (8) we can deduce that the magnetic field H_0 is correlated with the deformation between the neighboring particles Δd , which indicates that the relationship between the deformation and magnetic field strength is an increasing function. Insets 1, 2 and 3 of Fig. 2a show the photographs of the magnetic-induced deformation of MRE under the 0 mT, 100 mT and 200 mT respectively. As expected, the deformation of MRE film increased with increasing magnetic field strength. A qualitative fitting analysis was carried out in the supplementary content.

3.1.2 Mechanism of the TENG. The electric generation mechanism of the TENG is based on the coupling of contact triboelectrification and electrostatic induction, as illustrated in Fig. 2b. Because of the large composition percentage of fluorine that has the highest electronegativity among all elements, the FEP is one of the most triboelectric negative materials.⁴⁶ It always has a tendency to gain negative charges when in contacting with almost any other materials. Instead, the latex film over the surface of MRE

film contains the positive charge generally. In the absence of a magnetic field, no deformation occurs on the MRE film, and the gap between FEP and latex film is stable. The triboelectric charges on the surface of FEP and latex are balanced by their opposite counterparts, which would not to induce changes in the open-circuit voltage across the two electrodes. When an external magnetic field is applied to the TMFS, the magnetic-induced deformation of MRE would take the latex film close to FEP film. The electrostatic induction will cause the change in the open-circuit voltage across the two electrodes. The deformation and deformation rate of MRE film produced by which results in an electric output signal by TENG. The magnitude of the electric output signal is indicative of the local magnetic field. On the other hand, the magnitude of magnetic-induced deformation of MRE is strongly depending on the angle between the MRE film and magnetic field. As a consequence, the different angle would cause different electric output signal. This is the mechanism we will use in order to measure the intensity and direction of the UMF by detecting the electric output signal of TENG.

3.2 Magnetic-induced deformation character of the MRE film.

The magnitude of the deformation has been evaluated by the displacement of the center point in the rounded MRE film, which was detected by the laser range finder. The schematic diagram of the measurement system is shown in Fig. 3a. The UMF was generated with an electromagnet, and the strength can be

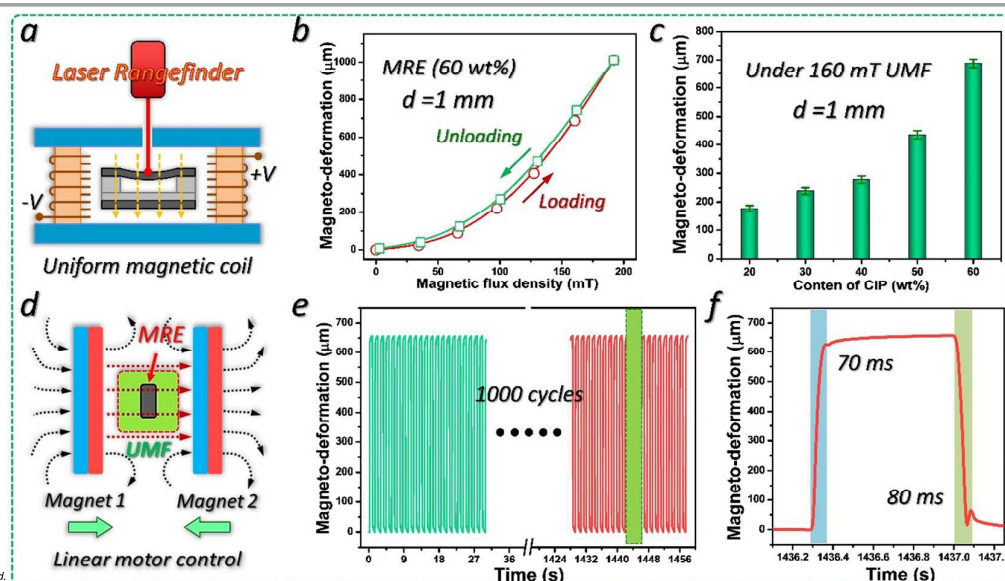


Fig. 3. Deformation performances of the MRE film in TMFS. (a) Schematic diagram of the measurement system for detecting the magneto-deformation. The UMF was generated with an electromagnet, and magnetic field strength can be controlled by the current I in the coil. The displacement of the center point in the rounded MRE film was detected by the laser rangefinder. (b) The curve of the magneto-deformation of MRE with the 60 wt% CIPs under the increasing and decreasing magnetic field strength. (c) The magneto-deformation of MRE with the different content of CIP under the 160 mT. (d) The schematic diagram of the measurement system for the deformation stability. The transient UMF was generated with two parallel magnets, which mounted on the slider of the guide rail. The displacement between the magnets was controlled by the linear motor, and the movement time of the slider is 50 ms. (e) The cycle tests of the magneto-deformation. The time for each cycle is 1s, and it includes the transient increase and decrease of the magnetic field. (f) A single-cycle curve of magneto-deformation, the response time has been marked.

controlled by the current I in the coil. The generated magnetic flux density B in the coil has been tested by teslameter, and the relationship between the continuously changing current and B was calculated by using the ANSYS software. Fig. 3b shows that the deformation initially increases slowly with increasing magnetic field strength, which can be attributed to the elastic interaction to resist deformation caused by the magnetic field. As the magnetic field continuously increasing, the deformation was found to exponentially increase with increasing magnetic field. It is also observed that the unload curve and the loading curve are almost consistent. It can be seen from Fig. 3c that the deformation has been enhanced by the increment of CIP content. It is primarily because of that the spacing of particles becomes smaller as the particle content increases. The enhanced magnetic interaction forces between the CIPs causes the larger deformation. Fig. S4a shows the curve of the magnetic-induced deformation of MRE with the different CIP content under the increasing and decreasing magnetic field strength. Obviously, the sample with the 60 wt% CIP has the highest sensitivity of the magnetic-induced deformation among the samples. Fig. S6a illustrates the influence of the MRE

film thickness on the deformation performance, and the deformation is increased with the decreasing thickness. Another phenomenon can be seen that the unloading curves are above the loading curves, this hysteretic effect can be attributed to the Mullins effect. Under tensile strain, the molecular chains of silicone rubber will be stretched and untwisted. The strain of molecular chains do not immediately recover in the unloading stage, which caused a larger deformation. The elastic restoring force has been reduced in the thin sample, which caused the obvious hysteretic effect. In order to achieve better stability, the MRE film with 1mm thickness has been chosen as the material components of the sensor device in the following section.

Deformation stability of MRE film has been tested by a measurement system based on the magnets and linear motor, the schematic diagram of the measurement system is shown in Fig. 3d. Through the cycle test, Fig. 3e shows an excellent deformation stability of MRE, which can be attributed to the excellent mechanical property of the MRE. The Fig. S6b shows the mechanical property of the MRE samples, the 60 wt% sample has the tensile

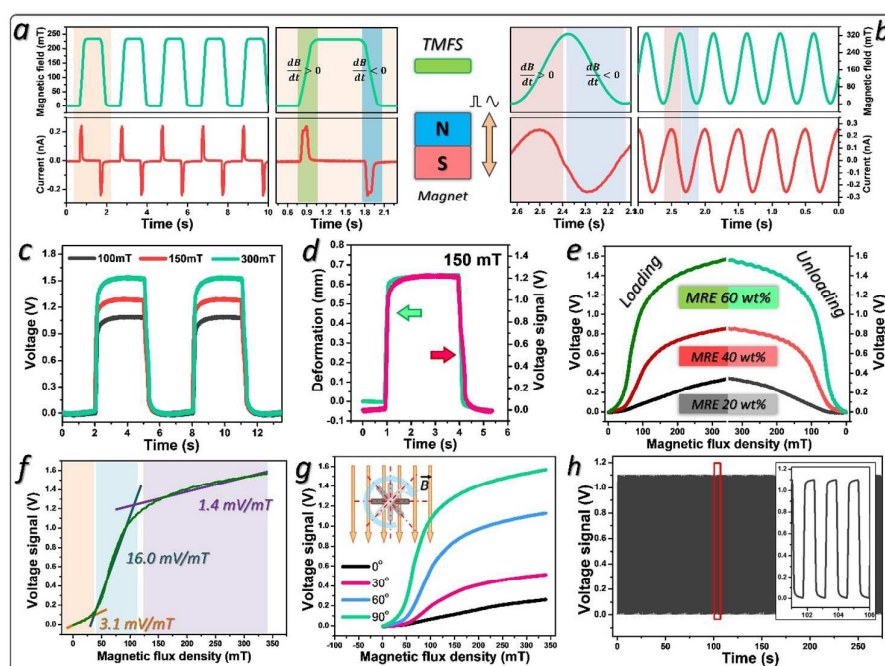


Fig. 4. Output performances of the TMFS for measuring strength and direction of magnetic field. (a) Cyclic changes of the magnetic field and the corresponding output current of the TMFS. Inset shows the schematic diagram of the measurement of time-varying magnetic field. The change and the changing rate of magnetic field is controlled by the movement of magnet. (b) Cyclic changes of the sinusoidal magnetic field and the corresponding output current of the TMFS. (c) Output voltage of TENG under the transient UMF with different strength. (d) The relationship between the deformation of MRE and the output voltage of TENG. (e) Output voltage of TENG under the uniformly increases and decreases UMF, the different curves corresponding to the MRE with changed content of CIP. (f) The different sensitivities of the TMFS with 60wt%-MRE in different stages, with a sensitivity of 3.1 mV/mT, 16 mV/mT, 1.4 mV/mT respectively. (g) Output voltage of TENG under the uniformly increases UMF, the different curves corresponding to the different angle between the MRE film and magnetic field. Inset shows the schematic diagram of the direction measurement of UMF, the sensor rotated with the magnetic field normal as the center axis, the angle between the MRE film and magnetic field is reduced from 90° to 0°. (h) The cycle test of output performances of the TMFS under the transient UMF. The time for each cycle is 1.5 s, and it includes the transient increase and decrease of the magnetic field.

strength of 1.09 MPa and breaking elongation of 580 %. Fig. 3b shows that the maximal magnetic-induced deformation of the MRE sample with 60 wt% CIPs is 1 mm, the corresponding stretch strain below 10%. It shows that the elastic strain of deformation is in the linear viscoelastic region, which ensured the stability and repeatability of the magnetic-induced deformation of MRE film in the following tests. Fig. 3f shows the response time of the magnetic-induced deformation, owing to the slider movement time is 50 ms, we can deduce that the response and reset time of the magnetic-induced deformation are about 20 and 30 ms, respectively.

3.3 Output performances of the TMFS.

To investigate the performance of the TMFS systematically, several parameters were discussed in both experimental and theoretical studies. Fig. 4a and Fig. 4b show the output current of the TMFS under different types (rectangle and sine) of time-varying magnetic field. It can be seen that the current outputs are generated when the magnetic field changed. The output current is positive when the magnetic field increases, and the output current is negative when the magnetic field decreases. The influences of the magnitude and frequency of the time-varying magnetic field on the output current of TENG are shown in the Fig. S7. These results are in good accordance with the output performance of the sensor designed by Yang *et al.*²⁷ It shows that TMFS can be used for the measurement of time-varying magnetic field.

Fig. 4c shows the voltage curves of TMFS under the transient UMF with different strengths. It can be observed that the response and reset of output voltage is almost instantaneous under the transient UMF, and the magnitude of output voltage increased with the increasing magnetic field strength. It can be attributed to the electrostatic induction between the FEP film and latex film, as discussed before. Larger deformation leads to smaller spacing between the FEP film and latex film, which caused a greater output voltage. Fig. 4d shows the relationship between the deformation of MRE and the output voltage of TENG, and the response shape of deformation are almost the same with that of output voltage. It reveals that the TMFS has an excellent response and recovery property, with the 20 ms response time and 30 ms reset time.

Fig. 4e shows the voltage curves of TMFS under the uniformly increased and decreased UMF, the loading curve and the unloading curve are almost symmetrical. It indicated the TMFS has the excellent stability under the different time-dependent UMF, which can be attributed to the excellent soft magnetic properties of CIP. In addition, Fig. 4e also reveals that the MRE film with higher CIP content in TMFS has the higher output voltage and detection sensitivity. These curves show some nonlinear characteristics, which can be attributed to the nonlinear relationship between magnetic-induced deformation and magnetic field strength. The output voltage initially increases slowly with increasing magnetic field strength, same as the deformation of MRE film. As the magnetic field strength reaches a threshold level, the output voltage of the TMFS was found to exponentially increase with

increasing magnetic field. Eventually, saturation phenomena are observed in the voltage curves under the high magnetic field.

As mentioned before, the curve of the TMFS with 60 wt%-MRE can be divided into three stages. Fig. 4f shows the different sensitivities of the TMFS with 60 wt%-MRE in these three stages, with a sensitivity of 3.1 mV/mT, 16 mV/mT, and 1.4 mV/mT respectively. By comparing the curves in Fig. 4e, it can be observed that the saturation strength decreased with the increasing CIP content, which provides a guidance of the material selection for the different measurement demand. Among them, the TMFS with the 60 wt%-MRE has a high sensitivity at the magnetic field ranges from 40 to 100 mT, and the TMFS with the 20 wt%-MRE has a high saturation strength. It mainly because of magnetic interaction of CIPs decreased with the decreasing CIP content. The smaller deformation result in the curve of the TMFS with the 20 wt%-MRE only shows the first stage in the test range. Among them, the TMFS with the 60 wt%-MRE has a high sensitivity at the magnetic field ranges from 40 to 100 mT, and the TMFS with the 20 wt%-MRE has a high saturation strength and better linearity. Fig. S8a reveals the influence of the gap between the upper part and lower part on the output voltage of TENG, the result indicated that the sensitivity and saturation strength has been reduced and enhanced with the increasing gap respectively.

The inset of Fig. 4g shows the schematic diagram of the direction measurement of UMF, and the change of the angle between the MRE film and magnetic field is obtained by rotating the TMFS with the magnetic field normal as the center axis. The output performance has been tested for the 90°, 60°, 30° and 0° respectively. Fig. 4g shows the different voltage response of TMFS under the increasing magnetic field with different directions, from which we can observe that the voltage is increased with the increasing angle. Fig. S8b shows the output voltage of TENG under the 150 mT transient UMF with the different angle. It also can be observed that the voltage is decreased with the decreasing angle. It's mainly because of CIPs tends to form a chain structure parallel to the direction of the magnetic field, and the movement trends decrease with the angle decreases. These angle-dependent output performances provide a viable method to detect the direction of the UMF. Finally, the continuous test has been carried out to investigate the stability of the output performance of TMFS, no obvious output change can be observed in the voltage curve, as shown in Fig. 4h.

4. Conclusions

In summary, we demonstrated a self-powered magnetic-field sensor for the sensing of time-varying and uniform magnetic field. In this design, the TENG has been used for detecting the deformation of MRE film, and the magnitude of electric output signal in TENG based on the electrostatic induction indicated the strength of the local magnetic field. Based on the excellent magnetic-induced deformation of MRE and the irreplaceable and unbeatable characteristics of TENG for perceiving the displacement changes, the designed TMFS shows high sensitivity and stability in the measurement of magnetic field.

The highest average sensitivity can be reached at 16 mV/mT, and the response time and reset time are about 20 and 30 ms, respectively. The results also show that the sensitivity of the sensor can be adjusted by MRE and device parameters. Finally, the direction measurement of UMF can be achieved based on the unique layer structure of TMFS. Our study suggests that the TMFS can be used for the magnetic-field measurements under no power condition with advantages of self-power, low cost, simple fabrication, rapid response and high sensitivity.

Acknowledgements

S. Q. and H. G. contributed equally to this work. Research supported by the Hightower Chair foundation, and the "thousands talents" program for pioneer researcher and his innovation team, China. This research is funded by the Equipment Research Joint Fund Project of Chinese Ministry of Education (grant No. 6141A02022108), Chongqing Research Program of Basic Research and Frontier Technology (Grant No. cstc2015jcyBX0069) and NSFC (51572040). The authors are grateful for the support.

Notes and references

Author Contributions

The manuscript was written through contributions of all authors. All authors have given approval to the final version of the manuscript.

Conflict of Interest: The authors declare no competing financial interest.

- S. A. Macintyre, *Electrical Measurement, Signal Processing, and Displays*, CRC Press, 2003.
- H. Emmerich and M. Schofthaler, *IEEE Trans. Electron Devices*, 2000, **47**, 972.
- Z. L. Wang, *Adv. Funct. Mater.*, 2008, **18**, 3553.
- S. Xu, Y. Qin, C. Xu, Y. Wei, R. Yang and Z. L. Wang, *Nat. Nanotechnol.*, 2010, **5**, 366.
- Z. L. Wang and J. Song, *Science*, 2006, **312**, 242.
- F.-R. Fan, L. Lin, G. Zhu, W. Wu, R. Zhang and Z. L. Wang, *Nano Lett.*, 2012, **12**, 3109.
- F.-R. Fan, Z.-Q. Tian and Z. L. Wang, *Nano Energy*, 2012, **1**, 328.
- L. Lin, S. Wang, S. Niu, C. Liu, Y. Xie and Z. L. Wang, *ACS Appl. Mater. Interfaces*, 2014, **6**, 3031.
- Z. L. Wang, *Mater. Today*, 2017, **20**, 74.
- Z. L. Wang, J. Chen and L. Lin, *Energy & Environmental Science*, 2015, **8**, 2250.
- H. Guo, J. Chen, Q. Leng, Y. Xi, M. Wang, X. He and C. Hu, *Nano Energy*, 2015, **12**, 626.
- H. Guo, Q. Leng, X. He, M. Wang, J. Chen, C. Hu and Y. Xi, *Adv. Energy Mater.*, 2015, **5**, 1400790.
- J. Chen, G. Zhu, W. Yang, Q. Jing, P. Bai, Y. Yang, T. C. Hou and Z. L. Wang, *Adv. Mater.*, 2013, **25**, 6094.
- Q. Liang, Z. Zhanga, X. Yan, Y. Gu, Y. Zhao, G. Zhang, S. Lu, Q. Liao and Y. Zhang, *Nano Energy*, 2015, **14**, 209.
- H. Guo, Z. Wen, Y. Zi, M. H. Yeh, J. Wang, L. Zhu, C. Hu and Z. L. Wang, *Adv. Energy Mater.*, 2016, **6**, 1501593.
- X. Zhong, Y. Yang, X. Wang and Z. L. Wang, *Nano Energy*, 2015, **13**, 771.
- G. Zhu, J. Chen, T. Zhang, Q. Jing and Z. L. Wang, *Nat. Commun.*, 2014, **5**, 3426.
- H. Guo, X. He, J. Zhong, Q. Zhong, Q. Leng, C. Hu, J. Chen, L. Tian, Y. Xi and J. Zhou, *J. Mater. Chem. A*, 2014, **2**, 2079.
- L. Zhang, B. Zhang, J. Chen, L. Jin, W. Deng, J. Tang, H. Zhang, H. Pan, M. Zhu and W. Yang, *Adv. Mater.*, 2016, **28**, 1650.
- J. Chen, J. Yang, Z. Li, X. Fan, Y. Zi, Q. Jing, H. Guo, Z. Wen, K. C. Pradel and S. Niu, *ACS nano*, 2015, **9**, 3324.
- Z. Wen, H. Guo, Y. Zi, M.-H. Yeh, X. Wang, J. Deng, J. Wang, S. Li, C. Hu and L. Zhu, *ACS nano*, 2016, **10**, 6526.
- X. Fan, J. Chen, J. Yang, P. Bai, Z. Li and Z. L. Wang, *ACS nano*, 2015, **9**, 4236.
- J. Jang, J. Lee, J. H. Jang and H. Choi, *Adv. Healthcare Mater.*, 2016, **5**, 2481.
- Y. Kim, J. Na, C. Park, H. Shin and E. Kim, *ACS Appl. Mater. Interfaces*, 2015, **7**, 16279.
- S. Wang, L. Lin and Z. L. Wang, *Nano Energy*, 2015, **11**, 436.
- X. Pu, H. Guo, J. Chen, X. Wang, Y. Xi, C. Hu and Z. L. Wang, *Sci. Adv.*, 2017, **3**, e1700694.
- Y. Yang, L. Lin, Y. Zhang, Q. S. Jing, T. C. Hou and Z. L. Wang, *ACS Nano*, 2012, **6**, 10378.
- M. Yu, S. Qi, J. Fu, P. A. Yang and M. Zhu, *Smart Mater. Struct.*, 2015, **24**, 045009.
- W. H. Li and M. Nakano, *Smart Mater. Struct.*, 2013, **22**, 055035.
- M. R. Jolly, J. D. Carlson and B. C. Munoz, *Smart Mater. Struct.*, 1996, **5**, 607.
- M. Yu, S. Qi, J. Fu, M. Zhu and D. Chen, *Compos. Sci. Technol.*, 2017, **139**, 36.
- Z. W. Xing, M. Yu, S. S. Sun, J. Fu and W. H. Li, *Smart Mater. Struct.*, 2016, **25**, 015026.
- M. Yu, P. Yang, J. Fu, S. Liu and S. Qi, *Smart Mater. Struct.*, 2016, **25**, 085046.
- Y. Wang, S. H. Xuan, B. Dong, F. Xu and X. L. Gong, *Smart Mater. Struct.*, 2016, **25**, 025003.
- Z. W. Xing, M. Yu, J. Fu, Y. Wang and L. J. Zhao, *J. Intell. Mater. Syst. Struct.*, 2015, **26**, 1818.
- J. Fu, P. D. Li, Y. Wang, G. Y. Liao and M. Yu, *Smart Mater. Struct.*, 2016, **25**, 035030.
- X. L. Gong, G. J. Liao and S. H. Xuan, *Appl. Phys. Lett.*, 2012, **100**, 211909.
- J. M. Ginder, S. M. Clark, W. F. Schlotter and M. E. Nichols, *Int. J. Mod. Phys. B*, 2002, **16**, 2412.
- X. C. Guan, X. F. Dong and J. P. Ou, *J. Magn. Magn. Mater.*, 2008, **320**, 158.
- W. Gao, L. L. Wang, X. Z. Wang and H. Z. Liu, *ACS Appl. Mater. Interfaces*, 2016, **8**, 14182.
- R. Fuhrer, C. M. Schumacher, M. Zeltner and W. J. Stark, *Adv. Funct. Mater.*, 2013, **23**, 3845.
- T. Kimura, Y. Umehara and F. Kimura, *Soft Matter*, 2012, **8**, 6206.
- Y. Shen, M. F. Golnaraghi and G. R. Heppler, *J. Intell. Mater. Syst. Struct.*, 2004, **15**, 27.
- G. T. Du and X. D. Chen, *Measurement*, 2012, **45**, 54.
- I. Bica and H. J. Choi, *Int. J. Mod. Phys. B*, 2008, **22**, 5041.
- Z. L. Wang, *ACS nano*, 2013, **7**, 9533.